

XMM-Newton Observation of IC 310 in the Outer Region of the Perseus Cluster of Galaxies

Kosuke SATO,¹ Tae FURUSHO,²
 Noriko Y. YAMASAKI,² Manabu ISHIDA,¹ Kyoko MATSUSHITA,³
 and Takaya OHASHI¹

¹*Department of Physics, Tokyo Metropolitan University,
 1-1 Minami-Osawa, Hachioji, Tokyo 192-0397
 ksato@phys.metro-u.ac.jp*

²*Institute of Space and Astronautical Science, Japan Aerospace Exploration Agency,
 3-1-1 Yoshinodai, Sagami-hara, Kanagawa 229-8510*

³*Department of Physics, Tokyo University of Science,
 1-3 Kagurazaka, Shinjuku-ku, Tokyo 162-8601*

(Received 2005 June 21; accepted 2005 August 24)

Abstract

We present results from an XMM-Newton observation of the head-tail radio galaxy IC 310 located in the southwest region of the Perseus cluster. The spectrum is well-fitted by an absorbed power-law model with a photon index of 2.50 ± 0.02 with no significant absorption excess. The X-ray image shows a point-like emission at IC 310 without any signs of a structure correlated with the radio halo tail. The temperature of the intracluster medium surrounding IC 310 declines as a function of distance from the cluster center, from $kT \sim 6$ keV in the northeast corner of the field of view to about 3 keV in the southwest region. Although we do not find any sharp edges in the surface brightness profile, a brightness excess over a smooth β model by about 20% is seen. The temperature also rises by about 10% in the same region. This indicates that the IC 310 region is a subcluster probably infalling into the Perseus cluster, and the gas in front of IC 310 towards the Perseus cluster is likely to be compressed by the large-scale motion, which supports the view that the IC 310 system is undergoing a merger.

Key words: galaxies: clusters: individual (Perseus) — galaxies: individual (IC 310) — galaxies: ISM — X-rays: galaxies — X-rays: ISM

1. Introduction

Recent imaging and spectral observations of clusters of galaxies by Chandra and XMM-Newton have significantly altered our view about clusters of galaxies. In particular, dynamical effects of infalling subgroups have been recognized in the form of cold fronts and shock fronts (e.g., 000 [cite]cite.Markevitch00Markevitch et al.(2000); Markevitch, Vikhlinin 2001; 000 [cite]cite.Vikhlinin01Vikhlinin et al.(2001)). In the Coma cluster, for example, an X-ray image showed gas heating between the NGC 4839 subcluster and the main cluster (000 [cite]cite.neumann01Neumann et al.(2001)). Such features clearly indicate that a subcluster merger is indeed taking place, and we can study how the gas is heated and how the extra energy is transferred into the surrounding space. High-sensitivity imaging spectroscopy of subclusters in the cluster outskirts will, therefore, produce important knowledge about the evolution of clusters.

IC 310 ($z = 0.0189$) is an S0 galaxy located in the southwest of the Perseus cluster ($z = 0.0183$) at an apparent distance of about ~ 1 Mpc from the cluster center. This galaxy is known as a head-tail radio galaxy (Sijbring, de Bruyn 1998), indicating that the radio lobe

with a length about 350 kpc ($15'$) is extended to the southwest direction, parallel to the line connecting IC 310 and the center of the Perseus cluster. This suggests that the galaxy may be moving toward the cluster center. de Bruyn and Brentjens (2005) have also detected significant polarized emission from a region close to IC 310 from low-frequency observations. te[cite]cite.schwarz92Schwarz et al.(1992) ([cite]cite.schwarz92Schwarz et al.(1992)) suggest a substructure around IC 310 from the PSPC image. An X-ray observation of IC 310 region is, therefore, an interesting case for studying any effect of subcluster motion on the ambient plasma around IC 310. The X-ray halo, if it is confirmed, can be used to probe the interacting features between the galaxy and the cluster gas.

The galaxy IC 310 also has its own scientific interest, such as time variability and Fe line feature. The luminosity measured by ROSAT (7.6×10^{42} erg s⁻¹, 000 [cite]cite.sambruna99Sambruna et al.(1999)) and ASCA ($\sim 10^{43}$ erg s⁻¹, 000 [cite]cite.furusho01aFurusho(2001)) suggests that this galaxy holds an active nucleus. Each spectrum was fitted well by a single power-law model with a spectral photon index of 3.7 and 2.1 with ROSAT and ASCA, respectively. The temperature map of the Perseus cluster obtained with ASCA showed an extended cool emission with $kT \sim 4$ keV around IC 310 (000

[cite]cite.furusho01bFurusho et al.(2001)).

This paper reports on the results from an XMM-Newton observation of the IC 310 region. We use $H_0 = 70 \text{ km s}^{-1} \text{ Mpc}^{-1}$, $\Omega_0=0.3$, $\Omega_\Lambda=0.7$ in this paper. At a redshift of 0.0189, $1'$ corresponds to 23.7 kpc.

2. Observation and Data Reduction

The XMM-Newton observation of IC 310 was carried out on 2003 February 26, for 29.4 ks. All of the EPIC cameras were operated in the full frame mode, and the medium filter for MOS and the thin filter for pn were used. Data reduction and analysis were performed by employing SAS version 6.0, CIAO 3.2, and HEASoft version 5.3.

Data of this observation obtained with XMM-Newton was affected by high-background flares. The data-cleaning method used in [cite]cite.reiprich04Reiprich et al.(2004) ([cite]cite.reiprich04Reiprich et al.(2004)) and Pratt and Arnaud (2002) were employed in event selection. First, we checked the light curves in the high-energy bands of 10–12 keV for MOS and 12–14 keV for pn, where the events were dominated by particle background due to soft protons. Good time intervals (GTIs) without background flares were selected from the light curves using conservative “generic cuts”, in which the count rate, C , was limited by $2.5(17.5) < C < 6.5(29.5) \text{ counts s}^{-1}$ for MOS(pn), respectively. Second, we applied the GTIs and selected the photon events with patterns 0–12 for MOS and 0–4 for pn, and flag = 0. We calculated the count-rate distribution with 100 s intervals, and then obtained new GTIs by requiring all of the count rates to be within $\pm 3\sigma$ around the mean. In this way, we iterated the process until the variation of the number of usable data in a step reached less than 5% compared with the previous value. The final count rates were 3.26–5.31 counts s^{-1} for MOS1, 3.10–5.04 counts s^{-1} for MOS2, and 19.3–27.9 counts s^{-1} for pn. After the above data selection, the remaining exposure times were 25.0, 24.9, and 19.2 ks for MOS1, MOS2, and pn, respectively.

We further needed to subtract the non X-ray background and the cosmic X-ray background (CXB). In a spectral analysis of IC 310, we used its outer annulus as the background, as described later. For analyzing the ICM, we used a background event data set created from blank-sky observations in Read and Ponman (2003). For the background files we applied the same selection criteria for the source event. The source-to-background count rate ratio was 0.90 for MOS1, 0.94 for MOS2, and 1.16 for pn calculated from the count rates in the 10–12 and 12–14 keV for MOS and pn. We rescaled the background spectra by rewriting the BACKSCAL header keyword according to these ratios (000 [cite]cite.fujita04Fujita et al.(2004)). Noting that the pn camera is considerably sensitive to background flares (000 [cite]cite.katayama04Katayama et al.(2004)), we therefore examined the results by changing the background normalizations by $\pm 10\%$ to assess any systematics uncertainties.

To make a correction for vignetting effects, the photon-weighting method of [cite]cite.arnaud01bArnaud et

al.(2001b) ([cite]cite.arnaud01bArnaud et al.(2001b)), as implemented in the SAS task “evigweight”, was applied to each source file and background file. For each event, this task computed the corresponding weight coefficient, defined as the ratio of the effective area at the photon position and the energy to the central effective area at that energy. When extracting spectra and images for specified energy bands, each event was weighted by this coefficient. Point sources were excluded by the SAS task “edetect” for all the event files. Throughout the paper we used the Galactic value of $N_H = 1.33 \times 10^{21} \text{ cm}^{-2}$ (Dickey, Lockman 1990) in the direction of IC 310 as the absorption for spectral analysis.

An X-ray image of the whole MOS and pn fields in the energy band of 0.5–10 keV is shown in figure 1. We made corrections for exposure and vignetting and adaptively smoothed the image. The gaps between the CCD chips are still seen in the image. The ICM emission is obviously brighter towards the center of the Perseus cluster, which is located in the northeast direction. The bright source at the center is IC 310, and apparently no X-ray halo or substructure is associated with the galaxy in the image.

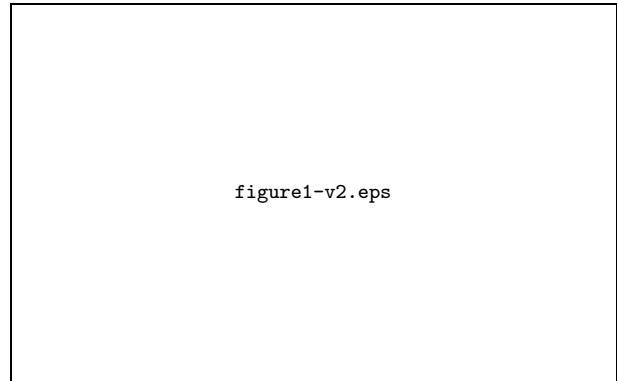


Fig. 1. Combined MOS + pn image of ICM around IC 310 in the 0.5–10.0 keV energy range. X-ray images and contours show adaptively smoothed, background subtracted, 0.5–10.0 keV MOS+pn images.

3. Result

3.1. IC 310

We first looked into IC 310 and its immediate region within a radius of $2'$. In this region, since the brightness variation is less than 5%, we can assume the ICM distribution to be uniform. The radial profile, centered on IC 310, for the MOS1 data of the exposure-corrected count rate in the energy band of 0.5–1 keV is shown in figure 2. The radial profile was fitted well with the Point Spread Function (PSF) and a constant, which was the sum of the NXB, CXB, and ICM emissions. Thus, the X-ray emission is considered to come from a point source, which is likely to be the central AGN of IC 310.

We extracted the source spectrum from the central circle with a radius of $2'$, and the background data were

taken from an annulus between radii of $2' - 4'$. The resulting spectra for the different instruments are shown in figure 3. The spectra of MOS1, 2, and pn were simultaneously fitted with an absorbed ($N_H = 1.33 \times 10^{21} \text{ cm}^{-2}$) power-law model. The best-fit photon index is 2.50, and the normalizations are consistent within 9% between the detectors. The obtained best-fit parameters are summarized in table.1. The flux and luminosity were taken from the results of MOS1, whose values are consistent with the past results obtained by ROSAT and ASCA (000 [cite]cite.sambruna99Sambruna et al.(1999); 000 [cite]cite.furusho01aFurusho(2001)). We derived an upper limit for the equivalent width of the neutral Fe line (6.28 keV at $z = 0.0189$) to be $EW < 180 \text{ eV}$ at the 90% confidence level. In order to examine the time variability of IC 310, we looked at the light curve for the data in the central $2'$ (radius) circle, as compared with those in the $2' - 4'$ annulus for the background. The count rate integrated over 2 ks showed no significant variation in excess of the statistical errors, which were about 5% at the 90% confidence level.

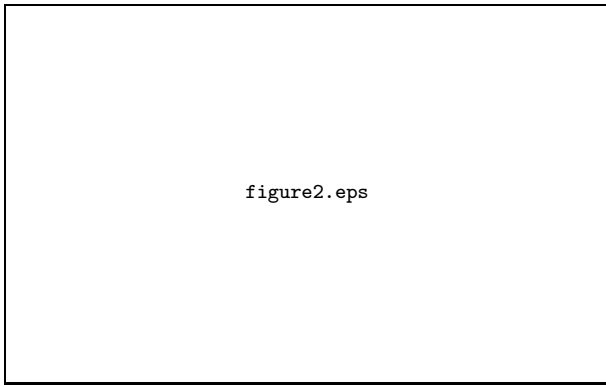


Fig. 2. Radial profile of IC 310. The MOS1 data were fitted with PSF and the background. The dotted and dashed curves show the background level and the profile of the point spread function (PSF), respectively, which are best fit to the radial profile. The solid curve is their sum.

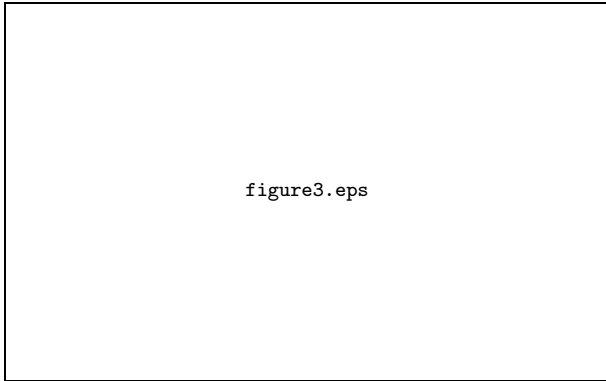


Fig. 3. X-ray spectra of IC 310 from MOS1 (black), MOS2 (red), and pn (green). The data were fitted well with an absorbed power law with a photon index of 2.50. The fit was carried out simultaneously with three cameras.

Table 1. Best-fit parameters of the spectral analysis of IC 310.

Parameters	MOS+pn
N_H (10^{21} cm^{-2})	1.33 (fixed)
photon index	$2.50^{+0.02}_{-0.02}$
reduced χ^2 (degrees of freedom)	1.12(688)
$F_X(0.5-2 \text{ keV})$ ($\text{erg cm}^{-2} \text{ s}^{-1}$)	$1.60 \times 10^{-12} *$
$F_X(2-10 \text{ keV})$ ($\text{erg cm}^{-2} \text{ s}^{-1}$)	$1.38 \times 10^{-12} *$
$L_X(0.5-2 \text{ keV})$ (erg s^{-1})	$2.05 \times 10^{42} *$
$L_X(2-10 \text{ keV})$ (erg s^{-1})	$1.14 \times 10^{42} *$
Fe line (EW) (eV)	< 180

All of the errors are at the 90% confidence level.

* The value obtained from MOS1; see text.

3.2. Intracuster Medium (ICM)

3.2.1. Surface brightness profile

The surface brightness profiles, plotted as a function of the distance from the center of the Perseus cluster, after point-source subtraction, are shown in figure 4 (a). The energy range is 0.5–10.0 keV. Events were binned in circular annuli centered at the X-ray emission peak of the center of the Perseus cluster. Background subtraction was carried out separately for each camera. The solid and dotted lines in figure 4 (a) indicate the best-fit 2- β model for the total cluster emission derived by [cite]cite.furusho01aFurusho(2001) ([cite]cite.furusho01aFurusho(2001)). The values of r_c and β were fixed at $r_{c1} = 10'.1$, $r_{c2} = 5'.0$, $\beta_1 = 0.64$, and $\beta_2 = 1.16$. Only the normalization was a free parameter. The difference between the data and the 2- β model suggests that the observed data are flatter in the range $25' - 30'$ and a small excess is seen in the $30' - 35'$ region. To look into the azimuthal dependence of the radial surface brightness profile, we divided the observed field into three evenly spaced sectors centered at the Perseus cluster center with an opening angle of 16° . The central line of the middle sector runs on IC 310. We compared the radial brightness profiles of these sectors, but no significant difference could be recognized in the intensity distribution for these 3 sectors.

3.2.2. Temperature profile from hardness ratio distribution

We produced a temperature map of the projected ICM structure using hardness ratios (HR). After point source and background subtractions, we produced images in two energy bands, 0.9–2.0 keV and 2.0–7.5 keV. HR is defined as the ratio of the counts between these bands. Since the events were corrected for the vignetting effect, the conversion factor from the HR to the temperature is the same throughout the image. We divided the region into $1.7' \times 1.7'$ cells for each image, took a running average of 2×2 cells, and then calculated the HR values. The temperatures were derived by the response matrices at the center of the field of view assuming an absorption of $N_H = 1.33 \times 10^{21} \text{ cm}^{-2}$ and a metal abundance of 0.3 solar. The temperature maps for the combined MOS data and the pn are shown in figure 5. In both maps, a temperature

drop is clearly seen from ~ 6 keV in the northeast region to ~ 3 keV in the southwest region. This feature is highly significant because statistical errors on the temperature are less than 10% in the observed field. The effect of the background was examined by changing the background normalizations by $\pm 10\%$ (see section 2). The obtained temperature values typically fluctuated by 10%, but the relation that the temperature dropped by half remained almost unaffected.

3.2.3. Radial profile of temperature

We also examined the radial profile of temperature along the direction towards the center of the Perseus cluster. The temperatures were calculated from HRs in the same manner as described in 3.2.2, but without taking running averages. The resulting profile is shown in figure 4 (b). The temperature declines by 30% from 6 keV at $r = 25'$ to 4 keV at $r = 45'$. As can be seen in the surface-brightness profile, a similar excess around $r = 35'$ is also noted in the temperature profile. We also examined the possible azimuthal dependence in the temperature profile in the same way as we did for the surface-brightness profile, but no significant difference was seen in the temperature profile over the statistical uncertainty, which is

on the order of $\sim 10\%$.

3.2.4. Temperature and abundance profile from spectral analysis

In order to obtain the temperature and metal abundance more accurately, we carried out spectral fits for each $4' \times 4'$ square region. The MOS and pn spectra were separately accumulated and fitted simultaneously with an absorbed MEKAL model, both in the 0.9–7.5 keV band in figure 6. The absorption was fixed at a Galactic value of $N_{\text{H}} = 1.33 \times 10^{21} \text{ cm}^{-2}$ in the direction of IC310. We show the resultant temperature map in figure 6, and the radial abundance profile in figure 8, respectively. The temperature map again indicates a drop from ~ 6 keV in the northeast region to ~ 3 keV in the southwest region, as can be seen in the map calculated from the HR (figure 5). The errors for the temperature are typically 20% at the 90% confidence level. When we varied the background normalization by $\pm 10\%$, the temperature relation between the northeast and the southwest regions was unaffected, as can be seen in section 3.2.2. We also found that the metal abundance declines from about 0.3 solar in the northeast region to about 0.15 solar in the southwest region. This feature is also statistically significant at the 90% confidence level. If these data points are tested against a constant-value model, we obtain a reduced $\chi^2 > 2$, whereas it reduces to about 1.3 for a linearly



Fig. 4. (a) Surface brightness profile, plotted as a function of the distance from the center of the Perseus cluster, in the 0.5–10.0 keV band. This profile was background subtracted and corrected for vignetting. The solid and dotted lines in the left figure are the best-fit 2β -model for each camera. (b) Temperature profile from the hardness ratio between the energy ranges, 2–7.5 and 0.9–2 keV, for MOS and pn for the ICM around IC 310.

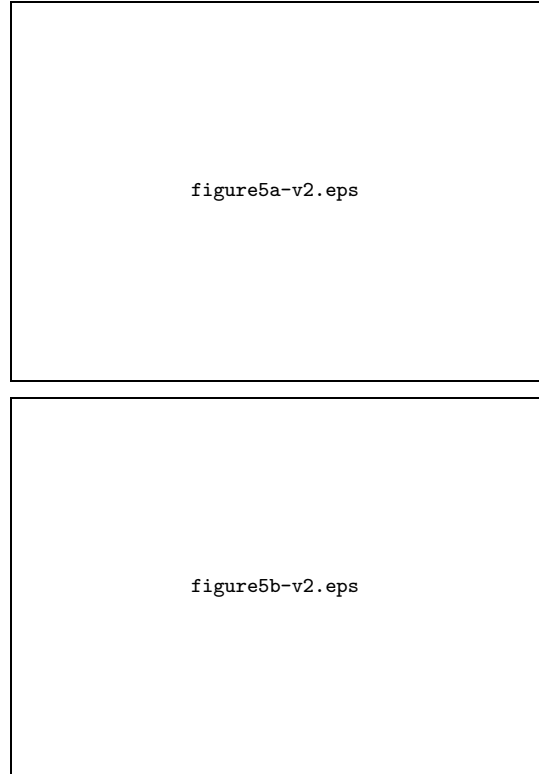


Fig. 5. Temperature maps obtained by MOS and pn overlaid with the same contour as in figure 1. The temperatures were calculated by HRs between below and above 2 keV. The red circles indicate the field of view of MOS.

declining model.

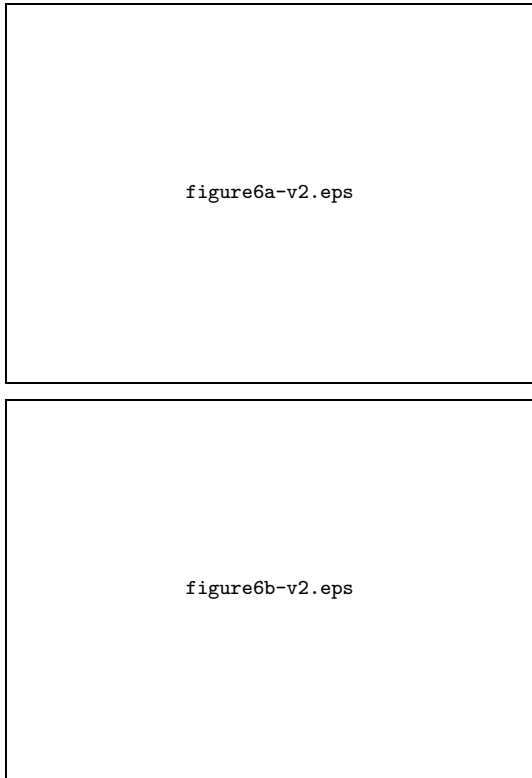


Fig. 6. Temperature map based on the spectral fit in the energy range 0.9–7.5 keV. The MOS and pn spectra were fitted with an absorbed MEKAL model. The red circle is the field of view of MOS.

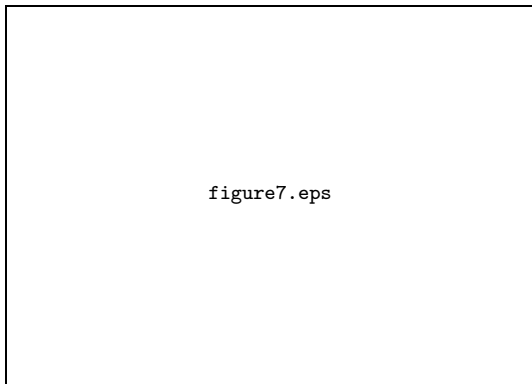


Fig. 7. X-ray spectrum of ICM around the 25' and the 45' region from the cluster center with pn camera. The data were fitted with the absorbed MEKAL model.

4. Discussion

4.1. IC 310

The X-ray radial profile of IC 310 was fitted well by the PSF of a point source. The energy spectrum was fitted with an absorbed power-law model with a rather

steep photon index of 2.5, and did not exhibit Fe lines ($EW < 180$ eV). These features indicate that the emission of IC 310 originates from the central AGN of the BL Lac-type object. However, the time variability was not detected during our observation, and the flux was consistent with the level measured during the past 10 yr by ASCA and ROSAT. We next estimated the possible X-ray emission from hot interstellar medium in the elliptical galaxy IC 310 based on the $L_X - L_B$ relation for elliptical galaxies (000 [cite]cite.canizares87Canizares et al.(1987); 000 [cite]cite.matsushita01Matsushita(2001); 000 [cite]cite.yamasaki02Yamasaki et al.(2002)). The optical luminosity of IC 310 was shown to be $L_B \sim 1 \times 10^{10} L_\odot$. This corresponds to an X-ray halo luminosity of $L_X \sim 10^{39} \text{ erg s}^{-1}$, which is three orders of magnitude lower than the that of the observed IC 310 value. This indicates that the X-ray emission of IC 310 is dominated by the AGN component, and the halo emission, if at all present, is masked by the PSF of the strong point-source emission. With much higher angular or spectral resolution, one may be able to detect the X-ray emission from a hot-halo associated with this galaxy.

VLA observations indicate a radio lobe in IC 310, and the radio flux densities at 49 cm $S_{49\text{cm}}$ are reported to be about 1.3 Jy (Sijbring, de Bruyn 1998). We looked into the radio lobe region reported in Sijbring and de Bruyn (1998), whose size is $15' \times 4'$, in the present field, and searched for any flux excess by comparing the flux with those in the immediate surrounding region. We detected no significant excess in the X-ray flux from the radio lobe; the upper limit is shown in table.2. If we assume that X-rays are emitted through the inverse Compton process with 2.7 K photons by the same relativistic electrons responsible for the radio lobe, the strength of the magnetic field is constrained. Following a prescription given by Harris and Grindlay (1979), we derived the lower limit of the magnetic field strength to be $B > 1\mu\text{G}$.

4.2. ICM around IC 310

The observed temperature in the present field is lower than the level at the central region of the Perseus

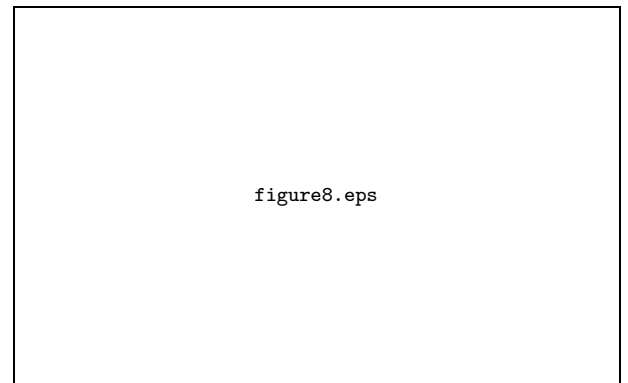


Fig. 8. Radial abundance profile from a spectral fit in 0.9–7.5 keV. The MOS and pn spectra were fitted with an absorbed MEKAL model. The solid line shows the best-fit linear model.

Table 2. Upper (lower) limits of the excess of the radio lobe region at the 2σ confidence level.

$F_X(0.5-10 \text{ keV}) [\text{erg cm}^{-2} \text{ s}^{-1}]$
$< 6 \times 10^{-14}$
$L_X(0.5-10 \text{ keV}) [\text{erg s}^{-1}]$
$< 5 \times 10^{40}$
Magnetic field $[\mu\text{G}]$
> 1

cluster, ~ 8 keV, excluding the cool core. The metal abundance is also lower than the central values of ~ 0.6 solar (000 [cite]cite.ezawa01Ezawa et al.(2001); 000 [cite]cite.churazov03Churazov et al.(2003)). The ICM temperature within the observed region also drops from ~ 6 keV at the northeast region to ~ 3 keV at the southwest region. These significant variations in the temperature and metal abundance confirm the results reported by [cite]cite.furusho01bFurusho et al.(2001) ([cite]cite.furusho01bFurusho et al.(2001)), who revealed the temperature gradient in the whole Perseus cluster based on ASCA observations. ASCA data indicated that the temperature in the west region of the Perseus cluster dropped from ~ 8 keV at ~ 0.5 Mpc from the center of the cluster to ~ 5 keV at ~ 1 Mpc. Some clusters were recently investigated as far as ~ 1 Mpc from the center; we note that in some systems (e.g., A 1413, A 478, A 2029, etc.), the temperature of ICM decreases by half from the peak location (usually around ~ 0.3 Mpc from the cluster center) to the ~ 1 Mpc region (000 [cite]cite.arnaud05Arnaud et al.(2005); 000 [cite]cite.pointecouteau05Pointecouteau et al.(2005); 000 [cite]cite.Vikhlinin05Vikhlinin et al.(2005)). Massive near-by clusters (e.g., the Coma cluster, the Virgo cluster) also show a temperature drop by $\sim 40\%$ from the central region to the ~ 0.5 Mpc region (000 [cite]cite.kikuchi00Kikuchi et al.(2000); 000 [cite]cite.arnaud01aArnaud et al.(2001a); 000 [cite]cite.shibata01Shibata et al.(2001)). The present case suggests that the infall of small and cool systems may be one of the possible causes of creating a lower ICM temperature in the outer region.

[cite]cite.schwarz92Schwarz et al.(1992) ([cite]cite.schwarz92Schwarz et al.(1992)) showed that the X-ray emission around IC 310 is more extended than that of a point source, when a smooth β -model was fitted and subtracted from a large-scale image, based on ROSAT observations. This implies that the IC 310 system is likely to be a subcluster or a group of galaxies. ASCA observations reveal a temperature drop at the region between the cluster center and IC 310 (000 [cite]cite.furusho01bFurusho et al.(2001)). These results suggest that the ICM in this region is subject to heating due to infall of the IC 310 system into the main Perseus cluster.

In the present observation, we did not detect any sharp structures, such as cold fronts or strong shock fronts in the X-ray image. We found, however, an excess of surface

brightness in the region between IC 310 and the center of the Perseus cluster, as shown in figure 4. A slight excess of the temperature is also seen in the same region. These features suggest that the ICM in this region is compressed by the pressure of the infalling gas associated with the IC 310 subcluster. The pressure, P , and the emissivity, I , can be expressed in terms of the electron density, n_e , and the temperature, T , as $P \propto n_e T$ and $I \propto n_e^2 \sqrt{T}$, which gives $P \propto I^{1/2} T^{3/4}$. The observed excess in the surface brightness around IC 310 is $\sim 20\%$, compared with the smooth β model profile for the whole cluster. The temperature excess is about 10% compared with the smooth trend of the temperature gradient in the present field of view. Thus, the pressure in this region is estimated to be 15% higher than the surrounding region.

We can break down the general merging process into two steps: first, the local temperature of the ICM is raised by shock heating or compression heating, and then the temperature of the whole cluster gradually increases due to growth of the gravitational potential after a merger. The observed small hump in the brightness and temperature around IC 310 suggests that the system is in a stage between the first and second steps. If the infall velocity of the subcluster is close to the sound velocity in the region of the pressure excess ($\sim 1200 \text{ km s}^{-1}$), the crossing time for a distance of 100 kpc ($4'$) is $\sim 1 \times 10^8 \text{ yr}$. In contrast, the time scale for thermalization of the whole Perseus cluster, estimated by the sound-crossing time over about 1 Mpc for a 5 keV plasma, is $\sim 10^9 \text{ yr}$.

5. Conclusions

We have presented the results from an XMM-Newton observation of the radio galaxy IC 310 and the surrounding ICM. The X-ray image of IC 310 is point-like, and the spectrum was fitted by an absorbed power-law model with a photon index of 2.50 ± 0.02 with no significant absorption at the source. An X-ray halo associated with this elliptical galaxy was not detected. No significant X-ray feature correlated with the radio halo extending in the southwest direction was seen, and we derived the lower limit for the magnetic field to be $> 1 \mu\text{G}$.

The emission from the ICM of the Perseus cluster filled the field of view of EPIC detectors, and we detected a systematic change of the temperature as a function of the distance from the center of the Perseus cluster, from $kT \sim 6$ keV in the northeast to ~ 3 keV in the southwest within the field of view. No sharp edges were seen in the brightness and temperature maps, but we recognized excess features in their radial profiles in the region between the center of the Perseus cluster and IC 310. In this region, the ICM is likely to be compressed by the infalling subcluster. The metal abundance in the ICM also decreases gradually from about 0.3 solar in the northeast region to about 0.1 solar in the southwest region.

The authors thank the referee for providing valuable comments. This research was supported in part by

Grants-in-Aid by the Ministry of Education, Culture, Sports, Science and Technology (14079103, 15340088). [Yamasaki et al.(2002)] Yamasaki, N. Y., Ohashi, T., & Furusho, T. 2002, ApJ, 578, 833

References

- [Arnaud et al.(2001a)] Arnaud, M., et al. 2001a, A&A, 365, L67
- [Arnaud et al.(2001b)] Arnaud, M., Neumann, D. M., Aghanim, N., Gastaud, R., Majerowicz, S., & Hughes, J. P. 2001b, A&A, 365, L80
- [Arnaud et al.(2005)] Arnaud, M., Pointecouteau, E., & Pratt, G. W. 2005, A&A in press
- [Canizares et al.(1987)] Canizares, C. R., Fabbiano, G., & Trinchieri, G. 1987, ApJ, 312, 503
- [Churazov et al.(2003)] Churazov, E., Forman, W., Jones, C., & Böhringer, H. 2003, ApJ, 590, 225
- [de Bruyn & Brentjens(2005)] de Bruyn, A. G., & Brentjens, M. A. 2005, A&A in press
- [Dickey & Lockman(1990)] Dickey, J. M., & Lockman, F. J. 1990, ARA&A, 28, 215
- [Ezawa et al.(2001)] Ezawa, H., et al. 2001, PASJ, 53, 595
- [Fujita et al.(2004)] Fujita, Y., Sarazin, C. L., Reiprich, T. H., Andernach, H., Ehle, M., Murgia, M., Rudnick, L., & Slee, O. B. 2004, ApJ, 616, 157
- [Furusho(2001)] Furusho, T. 2001, PhD Thesis, Tokyo Metropolitan University (ISAS RN-746)
- [Furusho et al.(2001)] Furusho, T., Yamasaki, N. Y., Ohashi, T., Shibata, R., & Ezawa, H. 2001, ApJ, 561, L165
- [Harris & Grindlay(1979)] Harris, D. E., & Grindlay, J. E. 1979, MNRAS, 188, 25
- [Katayama et al.(2004)] Katayama, H., Takahashi, I., Ikebe, Y., Matsushita, K., & Freyberg, M. J. 2004, A&A, 414, 767
- [Kikuchi et al.(2000)] Kikuchi, K., et al. 2000, ApJ, 531, L95
- [Markevitch et al.(2000)] Markevitch, M., et al. 2000, ApJ, 541, 542
- [Markevitch & Vikhlinin(2001)] Markevitch, M., & Vikhlinin, A. 2001, ApJ, 563, 95
- [Matsushita(2001)] Matsushita, K. 2001, ApJ, 547, 693
- [Neumann et al.(2001)] Neumann, D. M., et al. 2001, A&A, 365, L74
- [Pointecouteau et al.(2005)] Pointecouteau, E., Arnaud, M., & Pratt, G. W. 2005, A&A, 435, 1
- [Pratt & Arnaud(2002)] Pratt, G. W., & Arnaud, M. 2002, A&A, 394, 375
- [Read & Ponman(2003)] Read, A. M., & Ponman, T. J. 2003, A&A, 409, 395
- [Reiprich et al.(2004)] Reiprich, T. H., Sarazin, C. L., Kempner, J. C., & Tittley, E. 2004, ApJ, 608, 179
- [Sambruna et al.(1999)] Sambruna, R. M., Eracleous, M., & Mushotzky, R. F. 1999, ApJ, 526, 60
- [Schwarz et al.(1992)] Schwarz, R. A., Edge, A. C., Voges, W., Böhringer, H., Ebeling, H., & Briel, U. G. 1992, A&A, 256, L11
- [Shibata et al.(2001)] Shibata, R., Matsushita, K., Yamasaki, N. Y., Ohashi, T., Ishida, M., Kikuchi, K., Böhringer, H., & Matsumoto, H. 2001, ApJ, 549, 228
- [Sijbring & de Bruyn(1998)] Sijbring, D., & de Bruyn, A. G. 1998, A&A, 331, 901
- [Vikhlinin et al.(2001)] Vikhlinin, A., Markevitch, M., & Murray, S. S. 2001, ApJ, 551, 160
- [Vikhlinin et al.(2005)] Vikhlinin, A., Kravtsov, A., Forman, W., Jones, C., Markevitch, M., Murray, S. S., & Van Speybroeck, L. 2005, astro-ph/0507092